

Light extraction analysis and enhancement in a quantum dot light emitting diode

Ruidong Zhu, Zhenyue Luo, and Shin-Tson Wu*

CREOL, The College of Optics and Photonics, University of Central Florida, Orlando, Florida 32816, USA
*swu@ucf.edu

Abstract: We apply a rigorous dipole model to analyze the light outcoupling and angular performance of quantum dot light emitting diode (QLED). To illustrate the design principles, we use a red QLED as an example and compare its performance with an organic light emitting diode (OLED). By combining a high refractive index glass substrate with macroextractors, our simulation results indicate that the light outcoupling efficiency is doubled from ~40% to ~80%. After analyzing the light emission spectra and angular radiation pattern of the device, we confirm that QLED has a much weaker color shift than OLED.

©2014 Optical Society of America

OCIS codes: (230.5590) Quantum-well, -wire and -dot devices; (160.2540) Fluorescent and luminescent materials; (230.3670) Light-emitting diodes; (310.6845) Thin film devices and applications.

References and links

1. B. Geffroy, P. le Roy, and C. Prat, "Organic light-emitting diode (OLED) technology: materials, devices and display technologies," *Polym. Int.* **55**(6), 572–582 (2006).
2. C.-H. Hsiao, Y.-H. Lan, P.-Y. Lee, T.-L. Chiu, and J.-H. Lee, "White organic light-emitting devices with ultra-high color stability over wide luminance range," *Org. Electron.* **12**(3), 547–555 (2011).
3. S. Chung, J.-H. Lee, J. Jeong, J.-J. Kim, and Y. Hong, "Substrate thermal conductivity effect on heat dissipation and lifetime improvement of organic light-emitting diodes," *Appl. Phys. Lett.* **94**(25), 253302 (2009).
4. S. Reineke, M. Thomschke, B. Lüssem, and K. Leo, "White organic light-emitting diodes: status and perspective," *Rev. Mod. Phys.* **85**(3), 1245–1293 (2013).
5. C.-H. Chang, H.-C. Cheng, Y.-J. Lu, K.-C. Tien, H.-W. Lin, C.-L. Lin, C.-J. Yang, and C.-C. Wu, "Enhancing color gamut of white OLED displays by using microcavity green pixels," *Org. Electron.* **11**(2), 247–254 (2010).
6. A. Castan, H.-M. Kim, and J. Jang, "All-solution-processed inverted quantum-dot light-emitting diodes," *ACS Appl. Mater. Interfaces* **6**(4), 2508–2515 (2014).
7. K.-S. Cho, E. K. Lee, W.-J. Joo, E. Jang, T.-H. Kim, S. J. Lee, S.-J. Kwon, J. Y. Han, B.-K. Kim, B. L. Choi, and J. M. Kim, "High-performance crosslinked colloidal quantum-dot light-emitting diodes," *Nat. Photonics* **3**(6), 341–345 (2009).
8. V. Bulović, A. Shoustikov, M. A. Baldo, E. Bose, V. G. Kozlov, M. E. Thompson, and S. R. Forrest, "Bright, saturated, red-to-yellow organic light-emitting devices based on polarization-induced spectral shifts," *Chem. Phys. Lett.* **287**(3–4), 455–460 (1998).
9. L. Qian, Y. Zheng, J. Xue, and P. H. Holloway, "Stable and efficient quantum-dot light-emitting diodes based on solution-processed multilayer structures," *Nat. Photonics* **5**(9), 543–548 (2011).
10. B. Guzelturk, P. L. H. Martinez, Q. Zhang, Q. Xiong, H. Sun, X. W. Sun, A. O. Govorov, and H. V. Demir, "Excitonics of semiconductor quantum dots and wires for lighting and displays," *Laser Photonics Rev.* **8**(1), 73–93 (2014).
11. Y. Wang, V. D. Ta, Y. Gao, T. C. He, R. Chen, E. Mutlugun, H. V. Demir, and H. D. Sun, "Stimulated emission and lasing from CdSe/CdS/ZnS core-multi-shell quantum dots by simultaneous three-photon absorption," *Adv. Mater.* **26**(18), 2954–2961 (2014).
12. X. Yang, E. Mutlugun, C. Dang, K. Dev, Y. Gao, S. T. Tan, X. W. Sun, and H. V. Demir, "Highly flexible, electrically driven, top-emitting, quantum dot light-emitting stickers," *ACS Nano* **8**(8), 8224–8231 (2014).
13. Z. Luo, Y. Xu, and S.-T. Wu, "Emerging quantum-dots-enhanced LCDs," *J. Display Technol.* **10**(7), 526–539 (2014).
14. G. J. Supran, Y. Shirasaki, K. W. Song, J.-M. Caruge, P. T. Kazlas, S. Coe-Sullivan, T. L. Andrew, M. G. Bawendi, and V. Bulović, "QLEDs for displays and solid-state lighting," *MRS Bull.* **38**(09), 703–711 (2013).
15. Z. Luo, Y. Chen, and S.-T. Wu, "Wide color gamut LCD with a quantum dot backlight," *Opt. Express* **21**(22), 26269–26284 (2013).

16. J. F. Van Derlofske, J. M. Hillis, A. Lathrop, J. Wheatley, J. Thielen, and G. Benoit, "Illuminating the value of larger color gamuts for quantum dot displays," *SID Symp. Dig. Tech. Pap.* **45**(1), 237–240 (2014).
17. M. Sessolo and H. J. Bolink, "Hybrid organic-inorganic light-emitting diodes," *Adv. Mater.* **23**(16), 1829–1845 (2011).
18. H.-M. Kim, A. R. Mohd Yusoff, T.-W. Kim, Y.-G. Seol, H.-P. Kim, and J. Jang, "Semi-transparent quantum-dot light emitting diodes with an inverted structure," *J. Mater. Chem. C* **2**(12), 2259–2265 (2014).
19. B. S. Mashford, M. Stevenson, Z. Popovic, C. Hamilton, Z. Zhou, C. Breen, J. Steckel, V. Bulovic, M. Bawendi, S. Coe-Sullivan, and P. T. Kazlas, "High-efficiency quantum-dot light-emitting devices with enhanced charge injection," *Nat. Photonics* **7**(5), 407–412 (2013).
20. W. Brütting, J. Frischeisen, T. D. Schmidt, B. J. Scholz, and C. Mayr, "Device efficiency of organic light-emitting diodes: progress by improved light outcoupling," *Phys. Status Solidi A* **210**(1), 44–65 (2013).
21. R. Windisch, P. Heremans, A. Knobloch, P. Kiesel, G. H. Döhler, B. Dutta, and G. Borghs, "Light-emitting diodes with 31% external quantum efficiency by outcoupling of lateral waveguide modes," *Appl. Phys. Lett.* **74**(16), 2256–2258 (1999).
22. K. A. Neyts, "Simulation of light emission from thin-film microcavities," *J. Opt. Soc. Am. A* **15**(4), 962–971 (1998).
23. J. A. E. Wasey and W. L. Barnes, "Efficiency of spontaneous emission from planar microcavities," *J. Mod. Opt.* **47**(4), 725–741 (2000).
24. D. V. Talapin, J.-S. Lee, M. V. Kovalenko, and E. V. Shevchenko, "Prospects of colloidal nanocrystals for electronic and optoelectronic applications," *Chem. Rev.* **110**(1), 389–458 (2010).
25. W. K. Bae, S. Brovelli, and V. I. Klimov, "Spectroscopic insights into the performance of quantum dot light-emitting diodes," *MRS Bull.* **38**(09), 721–730 (2013).
26. W. K. Bae, Y.-S. Park, J. Lim, D. Lee, L. A. Padilha, H. McDaniel, I. Robel, C. Lee, J. M. Pietryga, and V. I. Klimov, "Controlling the influence of Auger recombination on the performance of quantum-dot light-emitting diodes," *Nat Commun* **4**, 2661 (2013).
27. M. K. Leung, W.-H. Yang, C.-N. Chuang, J.-H. Lee, C.-F. Lin, M.-K. Wei, and Y.-H. Liu, "1,3,4-Oxadiazole containing silanes as novel hosts for blue phosphorescent organic light emitting diodes," *Org. Lett.* **14**(19), 4986–4989 (2012).
28. S. Hofmann, M. Thomschke, B. Lüssem, and K. Leo, "Top-emitting organic light-emitting diodes," *Opt. Express* **19**(106), A1250–A1264 (2011).
29. H. P. Yoon, Y. Lee, C. D. Bohn, S.-H. Ko, A. G. Gianfrancesco, J. S. Steckel, S. Coe-Sullivan, A. A. Talin, and N. B. Zhitenev, "High-resolution photocurrent microscopy using near-field cathodoluminescence of quantum dots," *AIP Adv.* **3**(6), 062112 (2013).
30. E. D. Palik, *Handbook of Optical Constants of Solids* (Academic, 1985).
31. S. Nowy, B. C. Krummacher, J. Frischeisen, N. A. Reinke, and W. Brütting, "Light extraction and optical loss mechanisms in organic light-emitting diodes: Influence of the emitter quantum efficiency," *J. Appl. Phys.* **104**(12), 123109 (2008).
32. R. Meerheim, M. Furno, S. Hofmann, B. Lüssem, and K. Leo, "Quantification of energy loss mechanisms in organic light-emitting diodes," *Appl. Phys. Lett.* **97**(25), 253305 (2010).
33. D. Poitras, C.-C. Kuo, and C. Py, "Design of high-contrast OLEDs with microcavity effect," *Opt. Express* **16**(11), 8003–8015 (2008).
34. J.-H. Lee, K.-Y. Chen, C.-C. Hsiao, H.-C. Chen, C.-H. Chang, Y.-W. Kiang, and C. C. Yang, "Radiation simulations of top-emitting organic light-emitting devices with two- and three-microcavity structures," *J. Display Technol.* **2**(2), 130–137 (2006).
35. P. Yeh, *Optical Waves in Layered Media* (Wiley, 1988).
36. J. Zhao, J. A. Bardecker, A. M. Munro, M. S. Liu, Y. Niu, I. K. Ding, J. Luo, B. Chen, A. K. Y. Jen, and D. S. Ginger, "Efficient CdSe/CdS quantum dot light-emitting diodes using a thermally polymerized hole transport layer," *Nano Lett.* **6**(3), 463–467 (2006).
37. T. Tsutsui, "Progress in electroluminescent devices using molecular thin films," *MRS Bull.* **22**(06), 39–45 (1997).
38. S. E. Braslavsky, "Glossary of terms used in photochemistry, 3rd edition (IUPAC Recommendations 2006)," *Pure Appl. Chem.* **79**(3), 293–465 (2007).
39. O. Chen, H. Wei, A. Maurice, M. Bawendi, and P. Reiss, "Pure colors from core-shell quantum dots," *MRS Bull.* **38**(09), 696–702 (2013).
40. G. Horst, "Light extraction from organic light emitting diode substrates: simulation and experiment," *Jpn. J. Appl. Phys.* **46**(7A 7R), 4125–4137 (2007).
41. K.-Y. Chen, J.-H. Lee, M.-K. Wei, Y.-T. Chang, Y.-H. Ho, J.-R. Lin, and H. Y. Lin, "Device-dependent angular luminance enhancement and optical responses of organic light-emitting devices with a microlens-array film," *J. Soc. Inf. Disp.* **19**(1), 21–28 (2011).
42. S. Mladenovski, K. Neyts, D. Pavicic, A. Werner, and C. Rothe, "Exceptionally efficient organic light emitting devices using high refractive index substrates," *Opt. Express* **17**(9), 7562–7570 (2009).
43. C.-L. Lin, T.-Y. Cho, C.-H. Chang, and C.-C. Wu, "Enhancing light outcoupling of organic light-emitting devices by locating emitters around the second antinode of the reflective metal electrode," *Appl. Phys. Lett.* **88**(8), 081114 (2006).

44. J. Frischeisen, D. Yokoyama, A. Endo, C. Adachi, and W. Brütting, "Increased light outcoupling efficiency in dye-doped small molecule organic light-emitting diodes with horizontally oriented emitters," *Org. Electron.* **12**(5), 809–817 (2011).
45. P. Seong-Sik, S. Insung, C. Eunyong, P. Seungwon, and K. Euisoo, "Color shift reduction of liquid crystal displays by controlling light distribution using a micro-Lens array film," *J. Display Technol.* **8**(11), 643–649 (2012).
46. R. Lu, Q. Hong, Z. Ge, and S.-T. Wu, "Color shift reduction of a multi-domain IPS-LCD using RGB-LED backlight," *Opt. Express* **14**(13), 6243–6252 (2006).
47. C.-H. Oh, H.-J. Shin, W.-J. Nam, B.-C. Ahn, S.-Y. Cha, and S.-D. Yeo, "Technological progress and commercialization of OLED TV," *SID Symp. Dig. Tech. Pap.* **44**(1), 239–242 (2013).
48. C.-W. Han, K.-M. Kim, S.-J. Bae, H.-S. Choi, J.-M. Lee, T.-S. Kim, Y.-H. Tak, S.-Y. Cha, and B.-C. Ahn, "55-inch FHD OLED TV employing new tandem WOLEDs," *SID Symp. Dig. Tech. Pap.* **43**(1), 279–281 (2012).

1. Introduction

Organic Light-Emitting Diodes (OLEDs) have been widely used in smartphones and tablets [1], and general lighting [2]. However, OLEDs still suffer from a relatively short lifetime [3–5]. Under such circumstance, colloidal quantum dots (QDs) are emerging as a strong contender to overcome the lifetime issue because they are inorganic [6–10] and in the meantime QDs can be utilized for lasing applications [11]. Recently, the demonstration of a highly efficient top-emitting flexible QLED indicate that QLED is also catching up with OLED in the next generation flexible display [12]. Currently, two types of QD operation mechanisms have been realized: photoluminescence (PL) and electroluminescence (EL). The PL type is usually integrated into LCD backlight [13]. In this paper, we focus on the EL type, namely quantum-dot light emitting diode (QLED). The main differences between QLED and OLED are twofold: 1) QLED has symmetric and Gaussian-like emission spectra with a full width half maximum (FWHM) typically as narrow as 30 nm, while for OLED the spectrum is usually broader (~100nm) and more asymmetric [14]. Narrower emission spectra lead to a wider color gamut and more saturated colors [15, 16]. 2) In an OLED, all organic charge transport layers are the mainstream [17]; while in a QLED the hybrid organic-inorganic charge transport layers are preferred to ensure high efficiency [14, 18]. Because these inorganic materials, such as ZnO and TiO₂, usually have higher refractive indices than the organic layers [19], they will influence the light outcoupling of QLED structures.

A critical technical challenge of EL device is that its light output is affected by the External Quantum Efficiency (EQE); the highest EQE an EL device can achieve is limited by the light outcoupling efficiency of the device [2, 20, 21], which can be estimated from $1/(2n^2)$ for planar structures without outcoupling enhancement [22, 23], where n is the refractive index of the emitting material. For example, if the refractive index of the emitting medium is 1.7, then only ~17% of the total radiated power can be extracted out, while the remaining 83% is wasted and cannot be utilized. Such ceiling effect illustrates the importance for enhancing the light extraction of QLED structures.

Besides light outcoupling efficiency, the quantum yield of QD materials also plays an important role affecting EQE [24]. While the quantum yield of QLED is mainly determined by the material itself, the light outcoupling efficiency is primarily governed by the device structure. Presently many research efforts are focused on analyzing and improving the intrinsic quantum yield [9, 25, 26], there are few publications dealing with the outcoupling of QLED. However, if we trace back the LED and OLED development histories, in the beginning research is often concentrated on material exploration. But once the material development reaches a mature stage [27], more efforts are delved into device optimization [28]. QLED is expected to follow the same trend. Recently, a red QLED with 90% IQE has been demonstrated [19]. This IQE is comparable to that of the state-of-the-art OLED stacks, suggesting that the outcoupling efficiency will soon become the bottleneck of these highly efficient QLEDs. In this paper, we utilize the dipole model [22] to analyze the outcoupling of QLEDs. In the meantime, we discuss the light emission spectra, color shift, and angular

radiation pattern of the QLED structure. A well-known bottom-emitting OLED (BOLED) is used as benchmark for comparison.

2. Device structures

Figure 1(a) depicts the device structure of the inverted bottom-emitting QLED. It consists of a 40nm ITO (indium-tin-oxide) cathode, a 45nm zinc oxide electron-transporting layer (ETL), a 45nm cadmium selenide-cadmium sulfide (core-shell) quantum dot layer as the emitting layer (EML), a 65nm NPB hole transporting layer (HTL), a 15nm HAT-CN hole injection layer (HIL) and a 100nm Al anode. Such structure is similar to the structure proposed in [19], and we compare our numerical results to the experimental results reported in [19]. The intrinsic irradiance of the quantum dot layer is assumed to be the same as the PL spectra of the red quantum dots, as Fig. 1(b) shows, which is also taken from [19]. The emission is narrowband with FWHM~30 nm. The refractive indices of each layer are taken from literature [29–31].

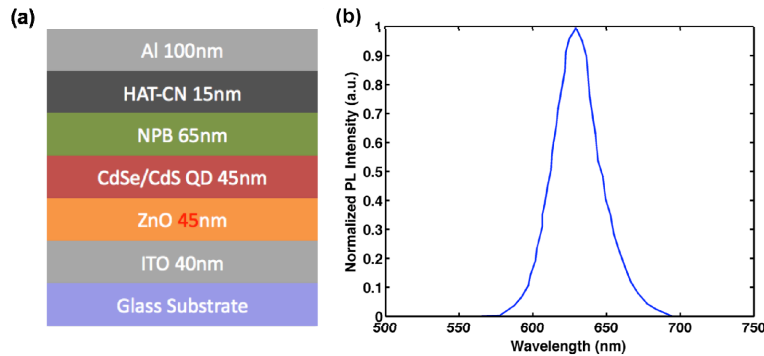


Fig. 1. (a) Structure of the proposed QLED stack and (b) PL spectra of the QDs taken from [19].

Figure 2(a) shows the BOLED structure. It consists of a 90-nm ITO anode, 60-nm NHT-5 doped with NDP-2 as HIL and HTL layer, 40-nm Cs-doped BPhen layer as electron injection layer (EIL) and ETL layer. To confine electrons in the EML layer, a 10-nm Spiro-TAD layer is used as the electron blocking layer (EBL) and a 10-nm BAQ layer as the hole blocking layer (HBL), the 20-nm EML layer consists of NPB doped with 10% Ir(MDQ)₂(acac). A 100-nm silver layer works as cathode. The PL spectrum of the material is shown in Fig. 2(b). This structure is well documented and discussed in [32], so we use it as benchmark for comparison.

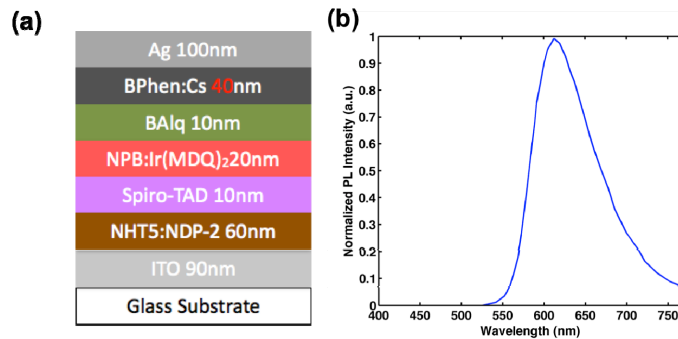


Fig. 2. (a) The device structure of the OLED stack and (b) the PL spectra of NPB:Ir(MDQ)₂(acac) taken from [32].

Before introducing our simulation model, we would like to mention that here we choose red QLED and OLED as examples because they have high IQE at contemporary stage, and

thus understanding the outcoupling of red QLED is urgent. For QLEDs with other colors, especially the blue QLED, they are still under active development stage and the IQE is still not high enough [25]. But our optical model can be extended to Blue QLED as well.

3. Simulation model

Two major approaches have been developed for simulating the emission properties of QLED: the simplified cavity model which describes the QLED structure as a Fabry-Pérot cavity [33, 34], and the more rigorous dipole model which describes the quantum dots as isotropic emitters within a multilayer medium. In both models, the multilayer structure is first simplified to a three-layer structure by the transfer matrix approach [35] to calculate the Fresnel coefficients of both top contact and bottom contact, as shown in Fig. 3; here $[R_T, T_T, A_T]$ and $[R_B, T_B, A_B]$ represent the [reflection, transmittance, absorption] of top and bottom contacts, respectively. For a bottom-emitting EL device, the transmittance of top contact is usually negligible, and a and b are the distance from emitter to top contact and bottom contact, respectively.

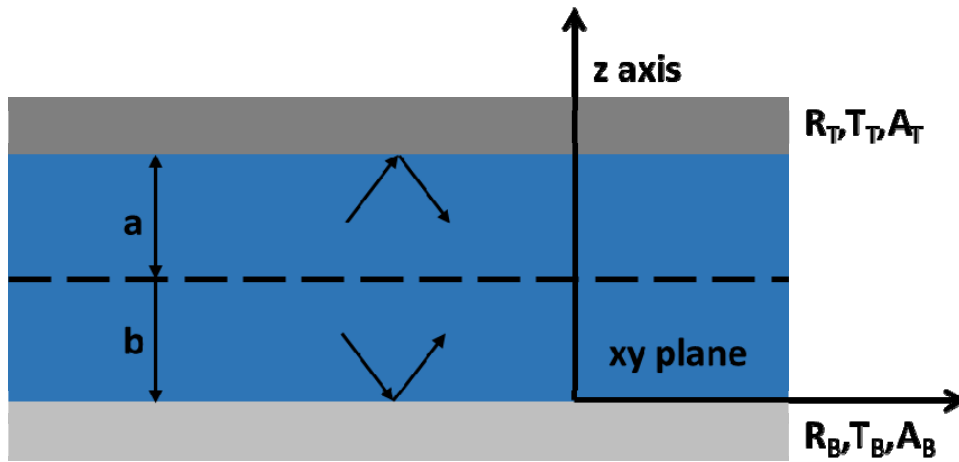


Fig. 3. Schematic drawing of the simplified three layer structure.

In the cavity model, the emitted irradiance can be expressed as [28, 33]:

$$I(\lambda, \theta) = \frac{1 + R_T + 2\sqrt{R_T} \cos(-\phi_T + \frac{4\pi n_e a \cos(\theta')}{\lambda})}{(1 - \sqrt{R_T R_B})^2 + 4\sqrt{R_T R_B} \sin^2(\frac{\Delta\phi}{2})} T_B I_0(\lambda). \quad (1)$$

In Eq. (1), λ is the emission wavelength, θ is the emitting angle in the air, θ' is the corresponding light propagation angle in the organic layer governed by the Snell's law, ϕ_T is the phase shift of the top contact, n_e is the refractive index of the organic material, $I_0(\lambda)$ is the intrinsic PL spectra of the QDs, and $\Delta\phi$ is the phase shift after one cycle, given by

$$\Delta\phi = \frac{4\pi n_e d \cos(\theta')}{\lambda} - \phi_B - \phi_T. \quad (2)$$

Again ϕ_B is the phase shift of the bottom contact. From Eqs. (1) and (2), we can calculate the irradiance spectra of the QLED structure [28].

Although the cavity model is adequate for simulating irradiance spectra and angular emission, it lacks the capability to determine the outcoupling efficiency of the QLED. On the

other hand, the dipole model can provide complete information in irradiance spectra, outcoupling efficiency as well as angular dependence [31]. Therefore, here we use the dipole model to evaluate the outcoupling efficiency and the corresponding loss channels of the QLED structure.

The dipole model was first developed to simulate the light emission spectra of OLED, in which the EQE is defined as [20]:

$$EQE = \eta IQE = \eta \gamma \eta_{S/T} q_{eff}, \quad (3)$$

where η is the outcoupling efficiency and IQE is the Internal Quantum Efficiency, which is the product of effective quantum yield q_{eff} , charge carrier balance γ , and singlet/triplet capture ratio $\eta_{S/T}$ [28].

Similar to OLED, the EQE of an QLED can be expressed as [20]:

$$EQE = \eta IQE = \eta \gamma q_{eff}. \quad (4)$$

In Eq. (4), we omit the singlet/triplet capture ratio term used in OLED because of the large spin-orbit coupling in QDs [36, 37]. The effective quantum yield q_{eff} of an QLED device is closely connected to the intrinsic quantum yield q , which can be further expressed as [25, 38]:

$$q = \frac{k_r}{k_r + k_{nr}}, \quad (5)$$

here k_r is the exciton radiative recombination rate and k_{nr} is the exciton non-radiative recombination rate.

Similarly, in the dipole model the QLED structure is also simplified to the equivalent three-layer structure shown in Fig. 3. And then the emissive QDs are treated as forced damped harmonic oscillators [22, 23]. The power generated by dipoles within a three-layer structure normalized to the power emitted in an infinite medium is given by [20]:

$$P = 1 - q + qF = 1 - q + q \int_0^{\infty} K(k_x) dk_x. \quad (6)$$

In Eq. (6), q is the intrinsic quantum yield of the QDs, F is the Purcell factor which describes how the cavity effect modifies the exciton recombination rate from k_r to k_r^* , K is the power dissipation density per unit dk_x , and k_x is the in-plane wave vector for waves propagating in the emitting medium. With Eq. (4) and Eq. (6), we can obtain the relation between q_{eff} and q :

$$\frac{q_{eff}}{q} = \frac{k_r^*}{k_r^* + k_{nr}} = \frac{F k_r}{F k_r + k_{nr}} = \frac{F}{qF + 1 - q}. \quad (7)$$

From Eq. (7), we see that the cavity can either increase or reduce q_{eff} with respect to q . Thus QLED stack design is not only important for the outcoupling of light emission, but also vital for enhancing the quantum yield of the QLED device if q is not equal to unity. How the cavity design influences the effective quantum efficiency has been described in detail in [32] and is beyond the scope of this paper. In this paper, our main purpose is to analyze the outcoupling of QLED, so we will assume $q = 1$ and $\gamma = 1$ if not otherwise specified.

Equation (6) is not explicit for calculating the power dissipation spectra and the outcoupling efficiency of the QLED, thus we need to express K explicitly. For the isotropic QDs, K consists of three terms [28]:

$$K = \frac{1}{3} K_{TMv} + \frac{2}{3} (K_{TMh} + K_{TEh}), \quad (8)$$

and

$$\begin{aligned}
K_{TMv} &= \frac{3}{2} \text{Re} \left[\frac{k_x^3 (1 + r_{TMv}^b e^{2ik_z b}) (1 + r_{TMv}^t e^{2ik_z a})}{k_e k_z^3 (1 - r_{TMv}^b r_{TMv}^t e^{2ik_z (a+b)})} \right], \\
K_{TMh} &= \frac{3}{4} \text{Re} \left[\frac{k_x k_z (1 - r_{TMv}^b e^{2ik_z b}) (1 - r_{TMv}^t e^{2ik_z a})}{k_e^3 (1 - r_{TMv}^b r_{TMv}^t e^{2ik_z (a+b)})} \right], \\
K_{TEh} &= \frac{3}{4} \text{Re} \left[\frac{k_x (1 + r_{TEv}^b e^{2ik_z b}) (1 + r_{TEv}^t e^{2ik_z a})}{k_e k_z (1 - r_{TEv}^b r_{TEv}^t e^{2ik_z (a+b)})} \right].
\end{aligned} \tag{9}$$

Here r is the reflection coefficient, subscripts v and h represent the dipoles parallel to the z axis and the x - y plane, respectively, TE and TM stand for transverse electric and transverse magnetic modes, $k_e = 2\pi n_e / \lambda$ is the wave vector of the emitting QD layer, $k_z = \sqrt{k_e^2 - k_x^2}$ is the wave vector along the z axis in the QD layer, and Re means the real part of the complex number.

From Eqs. (6)-(9), we can calculate the power dissipation spectra of the BOLED and the QLED structures. For example, Fig. 4 shows the power dissipation spectra of both BOLED and QLED at $\lambda = 620\text{nm}$ (the intrinsic quantum yield of both BOLED and QLED is assumed to be unity). From Fig. 4, we can determine from left to right the four optical channels of the BOLED and the QLED: direct emission, substrate mode, waveguide mode, and surface plasmons. These four channels are separated by their in-plane wave vector k_x . Details are described as follows: 1) Direct emission: $k_0 \cdot n_{air} \geq k_x \geq 0$, where $k_0 = 2\pi/\lambda$ is the vacuum wave vector, and n_{air} is the refractive index of air. Basically, the direct emission part is determined by the largest in-plane wavevector travelling at 90° in air. 2) Substrate mode: $k_0 \cdot n_{sub} \geq k_x > k_0 \cdot n_{air}$, where n_{sub} is the refractive index of glass substrate. In the substrate mode, the light experiences total internal reflection (TIR) at the substrate/air interface and is trapped inside the glass substrate. 3) Waveguide mode: $k_0 \cdot n_{eff} \geq k_x > k_0 \cdot n_{sub}$, where n_{eff} is the real part of the equivalent refractive index of the organic layers, QD layers and ITO layer (the metallic layer and the glass substrate layer are not included). The expression for n_{eff} is [20]:

$$\begin{aligned}
\varepsilon_{eff} &= \sum_i d_i / \sum_i (d_i / \varepsilon_i), \\
n_{eff} &= \text{Re}(\sqrt{\varepsilon_{eff}}).
\end{aligned} \tag{10}$$

In Eq. (10), d_i is the layer thickness, ε_i is the corresponding complex dielectric constant, and ε_{eff} is the equivalent dielectric constant. In this mode, light is guided inside the organic layers because of TIR at the ITO and glass interface. 4) Surface plasmons: $k_x > k_0 \cdot n_{eff}$, this mode corresponds to the evanescent wave at the QD/metal interface.

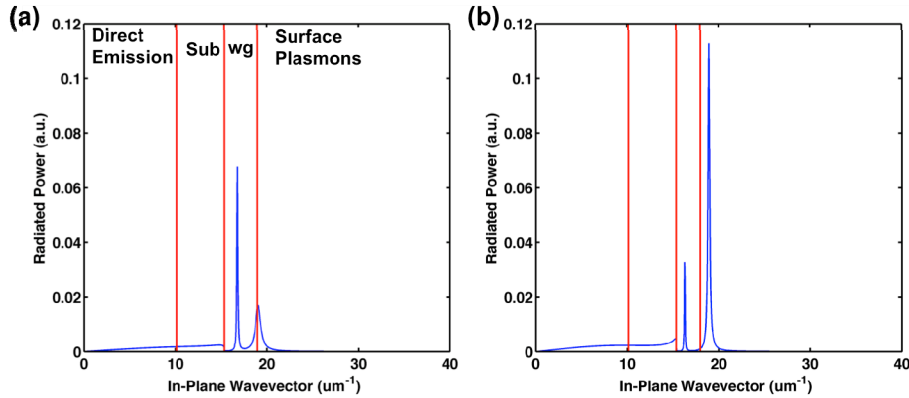


Fig. 4. Simulated power dissipation spectra of (a) QLED and (b) BOLED.

For the four optical channels, part of the dissipated power is absorbed inside the device instead of leaking into the corresponding optical channel, which is explained as follows: from Eq. (9), if k_z is real, then K_{TEh} can be rewritten as [22]:

$$\begin{aligned}
K_{TEh} &= \frac{3}{8} \frac{k_x}{k_e k_z} \left[\frac{|1 + r_{TEv}^b e^{2ik_z b}|^2}{|1 - r_{TEv}^b r_{TEv}^t e^{2ik_z (a+b)}|^2} (T_{TEv}^t + A_{TEv}^t) + \frac{|1 + r_{TEv}^t e^{2ik_z t}|^2}{|1 - r_{TEv}^b r_{TEv}^t e^{2ik_z (a+b)}|^2} (T_{TEv}^b + A_{TEv}^b) \right] \\
&= \frac{3}{8} \frac{k_x}{k_e k_z} \left[\frac{|1 + r_{TEv}^b e^{2ik_z b}|^2}{|1 - r_{TEv}^b r_{TEv}^t e^{2ik_z (a+b)}|^2} (T_{TEv}^t + T_{TEv}^b) + \frac{|1 + r_{TEv}^t e^{2ik_z t}|^2}{|1 - r_{TEv}^b r_{TEv}^t e^{2ik_z (a+b)}|^2} (A_{TEv}^t + A_{TEv}^b) \right] \quad (11) \\
&= K_{TEh}^T + K_{TEh}^A.
\end{aligned}$$

Here A and T represent the absorption and transmittance, respectively. K_{TMv} and K_{TMh} can also be treated similarly. With this approach, for non-evanescent waves, K can be separated into transmission part K^T and absorption part K^A , the transmission part is attributed to its corresponding optical channels while the absorption part is attributed to the intrinsic optical absorption, which comes from the intrinsic absorption of the organic and QD layers (for the organic and QD layers, the absorption coefficient κ is not equal to zero). With this approach, we can calculate the five optical channels inside the QLED: direct emission, substrate mode, waveguide mode, surface plasmons, and absorption.

Equation (6) only describes the power dissipation spectra at one wavelength. To calculate the entire spectra, Eq. (6) should be rewritten as follows by taking the normalized PL spectra $S(\lambda)$ into consideration [20]:

$$P = 1 - q + qF = 1 - q + q \int_{\lambda_1}^{\lambda_2} S(\lambda) \int_0^\infty K(k_x) dk_x d\lambda. \quad (12)$$

Equation (12) provides a way to calculate the total dissipated power of the QLED and the BOLED structure across the entire visible range (from $\lambda_1 = 400\text{nm}$ to $\lambda_2 = 800\text{nm}$).

Before we compare the QLED and the BOLED, we would like to emphasize that even though the two metallic electrodes used in QLED and OLED are different and they have different work functions, both of them can achieve high IQE (close to unity), as is demonstrated in [19] and [32], respectively. In our analysis we assume an IQE of unity to emphasize on the outcoupling properties of the devices, and thus the difference between a silver electrode and aluminum electrode is that their different refractive indices means different reflectivity of the top contact, which will finally affect the outcoupling of the QLED and the OLED. In our QLED and OLED structures, at the thickness of 100nm, both the silver electrode and the aluminum electrode are highly reflective. The similarity of the top contacts' reflectivity is the key issue why we can compare the QLED with the OLED even though they use different metals.

By analyzing the borders between different channels [32], it is possible to determine the ratio of different optical channels for the QLED and BOLED structures, as Fig. 5 illustrates.

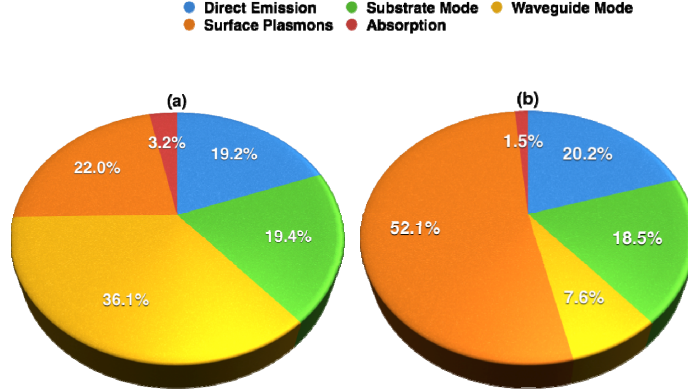


Fig. 5. Amount of power coupled to different optical channels for (a) QLED device and (b) BOLED device.

Without any additional outcoupling structure, only the direct emission part can be extracted. The relationship between directly emitted power P_{dir} and total radiated power P_{tot} is [20]:

$$q_{eff}\eta = P_{dir} / P_{tot}. \quad (13)$$

If we assume $q_{eff} = 1$, then it is simple to deduce from Fig. 5 that the EQE of QLED structure is 19.2%, which matches well the experimental results reported in [19], and this validates our model. Unlike its bulky counterparts, the solution-based CdSe/CdS thin films have a refractive index similar to that of the organic phosphors used in OLED. The relatively low refractive index of the thin films is mainly contributed by the organic ligands [39]. Thus, it is foreseeable that the EQE of the QLED is also limited by the EQE ceiling, which can be estimated as $1/(2n^2)$, where n is the refractive index of the CdSe/CdS layer.

For both the QLED and the BOLED, the direct emission part contributes to ~20% of the total radiated power. However, it is obvious that the waveguide mode in QLED contributes more to the total radiated power compared to BOLED (36.1% vs. 7.6%). The main reason for this enhanced waveguide mode is that the refractive index of the ZnO layer (~2.0) is larger than that of the organic layer (~1.8) [18]. Thus, the waveguiding effect between the glass substrate and the QLED stacks is stronger than that of the OLED structure with all organic layers. Such a difference in waveguide mode contribution has potential applications for enhancing the outcoupling of the QLED structure. To fully understand the difference, we have to examine the power dissipation spectra across the whole visible range, as shown in Fig. 6. The four regions in the figure are: 1) Direct emission, 2) Substrate mode, 3) Waveguide mode, and 4) Surface plasmons. The red line represents $k_{air} = k_0 \cdot n_{air}$, green $k_{sub} = k_0 \cdot n_{sub}$, and white $k_{eff} = k_0 \cdot n_{eff}$. It is obvious that for the QLED in Fig. 6(a), a large portion of the power is dissipated evenly in the waveguide mode and surface plasmons, while for BOLED [Fig. 6(b)] it is obvious that there are two distinct modes in regions 3 and 4, and the surface plasmons are much stronger than the waveguide mode. These mechanisms contribute to the much stronger waveguide mode in the QLED.

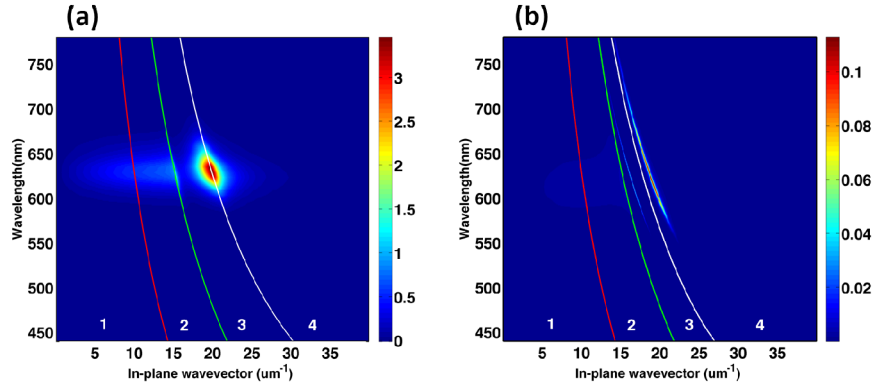


Fig. 6. Simulated full power dissipation spectra of (a) QLED and (b) BOLED.

4. Optimization of QLED device structure

As explained above, the EQE of QLED is limited by the direct emission part so that it is of vital importance to extract or reduce other optical modes. Currently, a few approaches [36–40] have already been proposed to extract/reduce the other optical modes in an OLED structure. Because of the similarity between QLED and OLED, most of them will also work for QLED, although their contribution or enhancement factor may be different.

To extract substrate mode, the most straightforward approach is to use macroextractors such as hemispheres to circumvent the TIR at the substrate/air interface [40]. The substrates with microstructures such as microspheres and micropyramids can also be used to extract the substrate mode [41]. As explained in [4], for the hemisphere-type macroextractors, all the light trapped in the substrate mode can be outcoupled as the light is at normal incidence when entering the glass hemisphere. Whereas for the case of microstructures, it has been explained in [40] that the aspect ratio and density of the microstructures greatly affect the outcoupling efficiency of the device, and thus it is difficult to outcouple the entire substrate mode. Overall it is safe to say that with the macroextractors, the EQE ceiling of the QLED device has been pushed to a larger portion, with both the light directly emitted and the light previously trapped inside the glass substrate.

As for the waveguide mode, the most straightforward way is to use high refractive index glass substrate, thus the light is trapped inside the substrate instead of the organic and ITO layers [42]. Subsequently, the substrate mode can be extracted further by the macroextractors. We will discuss more about this approach later.

The most difficult mode to extract is the surface plasmons, as it leaks into the metallic electrode as evanescent wave. Thus, the main effort is to reduce the transition to surface plasmons instead of extracting them. The main approach to reduce the surface plasmons is to fine-tune the distance between the emitting layer and the metallic electrode. However, this approach usually comes with increased waveguide mode ratio [43]. At the same time, in OLED stacks the surface plasmons can be suppressed by using oriented emitters [44], while for QLED this is not the case as QDs are isotropic.

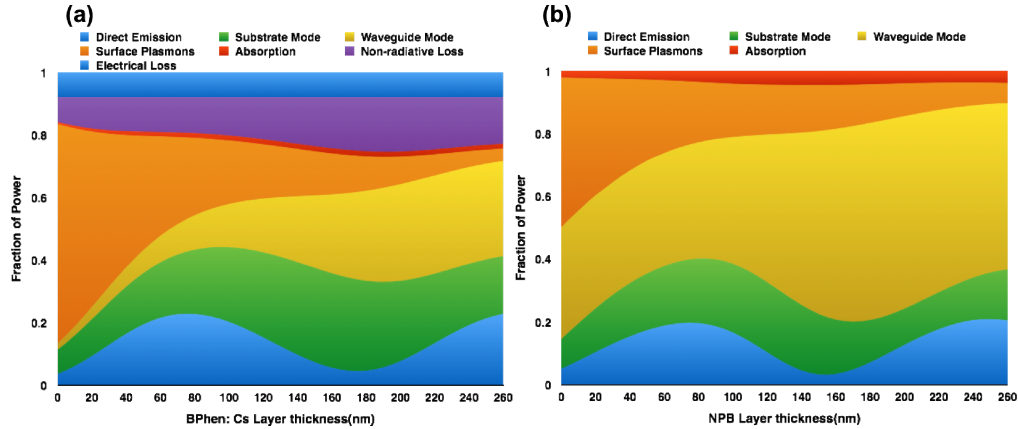


Fig. 7. (a) Changing the proportions of different optical channels by tuning the BPhen:Cs layer thickness for the OLED structure, and (b) Changing the proportions of different optical channels by tuning the NPB layer thickness for the QLED structure.

Among all these approaches, the most straightforward and economic way to enhance light outcoupling is to optimize the QLED stack by varying the layer thickness. For example, Fig. 7(a) shows the contributions of different optical channels as a function of the BPhen:Cs layer thickness for the BOLED structure with the assumption that $q = 0.84$ and $\gamma = 0.92$. The results agree well with the experimental data reported in [32], which confirms the validity of our simulation model. Similarly, we can use this optimization approach for the QLED stack, Fig. 7(b) shows the corresponding results by varying the thickness of the NPB (HTL) layer, this time a unity intrinsic quantum yield is assumed. From Fig. 7(b), it is obvious that as the NPB layer is between the Al anode and the emitting layer, the variation of NPB layer thickness greatly modifies the OLED cavity, as can be seen from the oscillation of the direct emission part. And it is obvious that the coupling to the surface plasmons is mainly determined by the distance from the emitting layer to the metallic electrode. Thus, increasing the NPB layer thickness greatly reduces the surface plasmons mode. However, the reduced surface plasmons mode mainly transfers to the waveguide mode; the direct emission mode and the substrate mode are still limited by the EQE ceiling. At 75nm, the direct emission reaches the maximum value of 22.8%, while at 95nm direct emission and substrate mode sum up to the maximum of 44.1%. This means that even with outcoupling enhancing structures, at the most only a little less than half of the emitted light can be extracted.

If we vary the ZnO (ETL) layer thickness, the results are a little bit different, as Fig. 8 depicts. This time the cavity effect is much weaker as the thickness between the emitting layer and the metallic electrode is not changed, still it is obvious that only about 40% of the light can be extracted even with outcoupling structures. Without the outcoupling structures, at the most only about 20% of the light can be extracted.

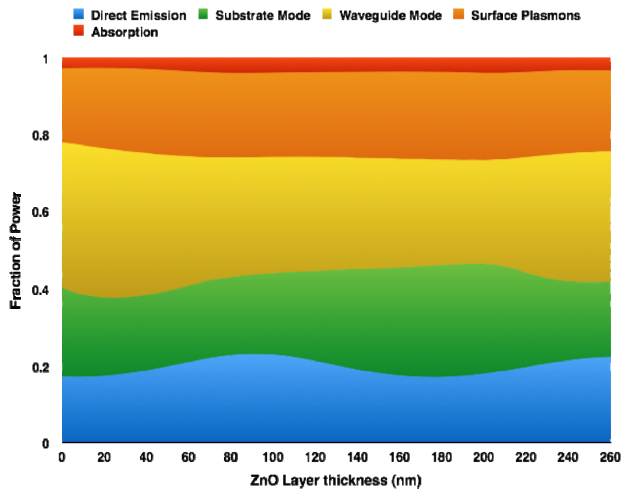


Fig. 8. Changing the fraction of power of different optical channels for the QLED structure by varying the ZnO layer thickness.

Of course we can also vary the thickness of the HAT-CN layer, the ITO layer or vary the thickness of two layers simultaneously to optimize the QLED structure, but our tedious optimization of other layer thickness, which is not listed here, indicates that the maximum outcoupling efficiency is still governed by the EQE ceiling. And QLED stack optimization by varying the layer thickness alone is insufficient to dramatically enhance the outcoupling efficiency. Thus, additional approach is required. As mentioned before, generally, it is assumed that with outcoupling structures such as macroextractors, all the direct emission part and the substrate mode can be extracted. The simplest way to enhance the outcoupling of both direct emission and substrate mode is to use a high refractive index glass substrate to reduce or even eliminate the waveguide mode. As demonstrated in Fig. 5, compared to BOLED the QLED structure has more contributions from the waveguide mode. Thus, it is more rewarding to utilize high refractive index glass substrate modes in QLED stack. For example, if we replace the BK7 glass substrate with a glass substrate with $n = 1.8$, then the ratio of different optical channels is shown in Fig. 9.

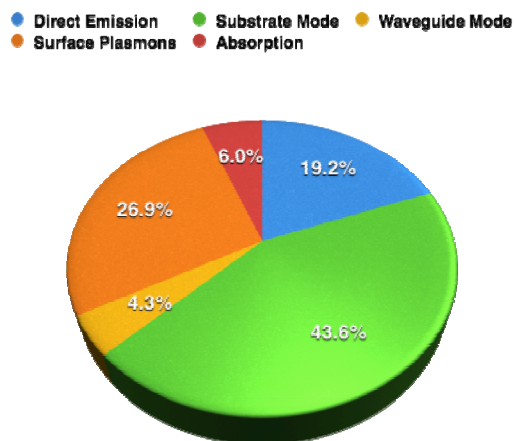


Fig. 9. Amount of power coupled to different optical channels for the QLED device with a high refractive index ($n = 1.8$) substrate.

As expected, the direct emission part and substrate mode together now accounts for 62.8%, and the waveguide mode is reduced to 4.3%. If the refractive index of the glass

substrate is further increased, the waveguiding effect can be fully eliminated. Table 1 summarizes the fraction of power coupled to different modes for the QLED stack with substrate having different refractive indices. From Table 1, as the refractive index of the substrate increases, the waveguide mode can be fully suppressed. However, after the waveguide mode is suppressed, further increasing the substrate refractive index does not help much about extracting more direct emission part and substrate mode, because the absorption from the multilayer structure becomes more severe. For different substrate refractive index, we can optimize the structure by tuning the layer thickness. Figure 10 shows the maximum fraction of power for both direct emission part and substrate mode we can get by tuning the HTL layer thickness (up to 260nm) under different substrate refractive indices. As Fig. 10 shows, it increases with the substrate refractive index and then saturates. Considering the high cost of high refractive index glasses, the optimal refractive index of glass should be around 2.0. From Fig. 10, we can see that at the most we can extract ~80% of the total emitted power by using high refractive index substrate and outcoupling structures. That is about 2X improvement compared to the structures with BK7 glass if we count both direct emission part and substrate mode. As surface plasmons mode is also greatly reduced when we use high refractive index substrate, the bottleneck comes from the absorption of the QLED structure, which is attributed to the high reflectivity of the substrate.

Table 1. Fractions of power coupled to different modes for the QLED stack with substrates having different refractive indices.

Substrate	Direct Emission	Substrate Mode	Waveguide Mode	Surface Plasmons	Absorption
BK7($n \approx 1.5$)	19.2%	19.4%	36.1%	22.0%	3.2%
$n = 1.8$	19.2%	43.6%	4.3%	26.9%	6.0%
$n = 2.0$	19.0%	59.3%	0.0%	5.6%	16.1%
$n = 2.2$	18.7%	62.0%	0.0%	2.4%	16.9%
$n = 2.4$	18.3%	62.6%	0.0%	1.6%	17.5%

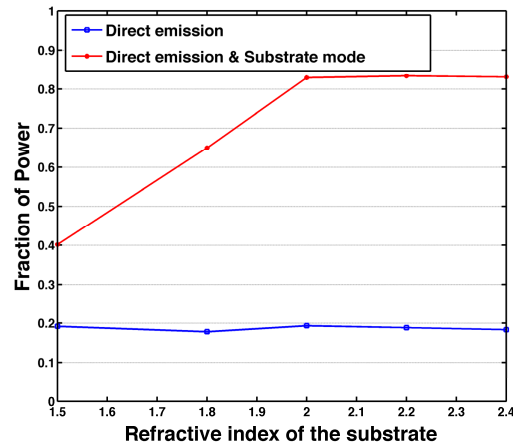


Fig. 10. How the refractive index of the substrate affects different optical channel power proportion.

To fully understand the power redistribution because of the high refractive index substrate, we examine the power dissipation spectra of the QLED with different substrate refractive index [Fig. 11]. From Figs. 11(b)-11(d), as n_{sub} is larger than n_{eff} , waveguide mode vanishes.

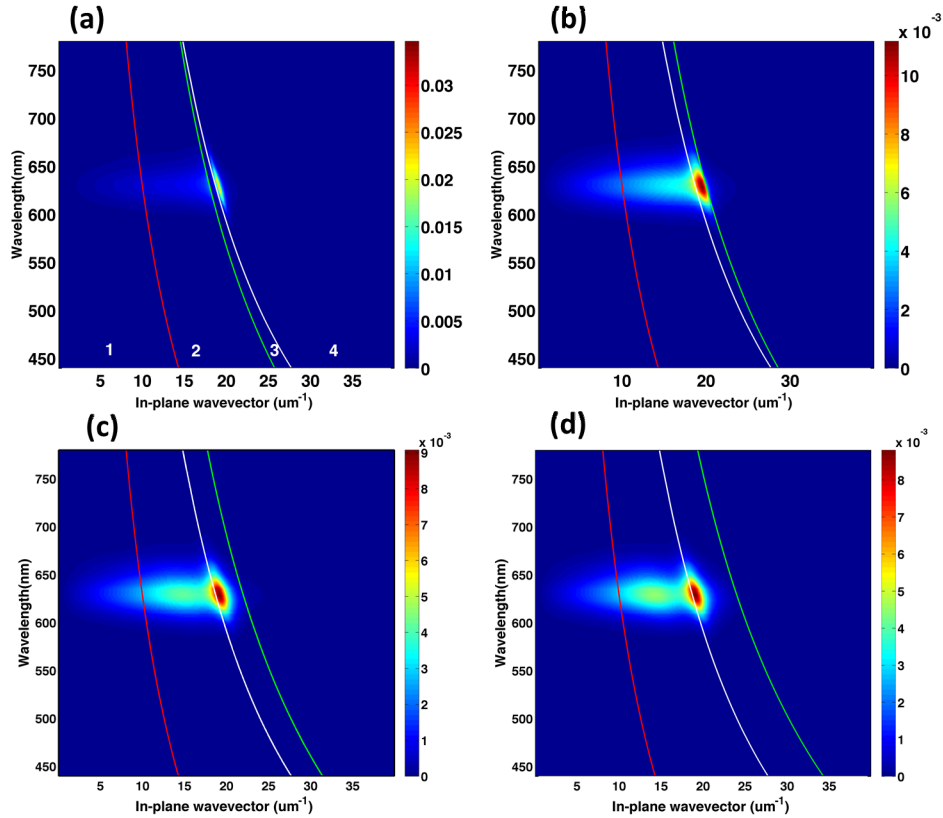


Fig. 11. Full power dissipation spectra of the QLED with different substrate refractive indices: a) $n_{sub} = 1.8$ b) $n_{sub} = 2.0$ c) $n_{sub} = 2.2$ d) $n_{sub} = 2.4$.

This is indicated by the white line representing $k_{eff} = k_0 \cdot n_{eff}$, which is smaller than the green line representing $k_{sub} = k_0 \cdot n_{sub}$, illustrating that the waveguide mode has vanished entirely and transferred to substrate mode and surface plasmons. With Fig. 11 we are also able to explain why surface plasmons first increase a little bit and then decrease dramatically. As n_{sub} increases, the waveguide mode is transferred to the substrate mode. At first as n_{sub} is still not large enough, there is still much portion of the energy left in the surface plasmons, the factors add up to the increased surface plasmons, however, with the continuing increase of n_{sub} , more and more energy is transferred to substrate mode, and when $n_{sub} > n_{eff}$, the conditions for surface plasmons are modified to $k_x > k_0 \cdot n_{sub}$, which accounts for smaller part of the total dissipated power as indicated by the green lines in Fig. 11.

5. Analyzing the light emission pattern

Besides outcoupling efficiency, light emission pattern is also important for display and lighting applications. Using the dipole model, it is also possible to calculate the light emission pattern of the QLED and the OLED structures shown in Fig. 1(a) and Fig. 2(a), respectively. The simulated results are shown in Fig. 12. It is evident that the light emission spectrum of the QLED structure (~30nm) is much narrower than that of the OLED structure (~80nm). This means we can get much purer and more saturated color from the QLED structure.

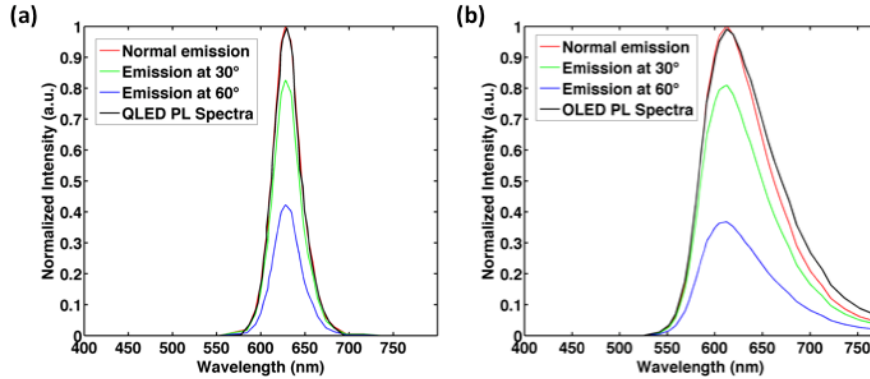


Fig. 12. Emission spectra of the (a) QLED stack (b) BOLED stack.

If we compare the EL spectra of the QLED/BOLED with its PL spectra, we can see that the cavity effect will modify the spectra of the inhomogeneously broadened emission spectra of the QD/Organic ensembles. As these two devices are both bottom emitting devices with low reflectivity and relatively high transmittance on the bottom side, such modification is not very noticeable for the two devices, especially for the QLED device as its PL spectra is already very narrow. This effect will also modify the emission spectra for Green QLED and Red QLED, and will be different for them because of the intrinsically inhomogeneously broadened spectra.

Generally speaking, QLED has narrower emission linewidth than OLED; therefore, QLED should have much smaller color shift at oblique angles than OLED. This is indeed confirmed by the $\Delta u'v'$ diagram plotted in Fig. 13. Our red QLED has a $\Delta u'v'$ less than 0.002, which is much smaller than that of a film-compensated multi-domain vertical-alignment LCD panel [45], whose $\Delta u'v'$ is 0.005 for the same color. The main reason for this smaller color shift is that QLED does not have birefringence as liquid crystals do [46]. As for the OLED structure, the color shift of the red color is ~ 0.01 , which is comparable with commercial OLED products [47, 48], but is still much higher than QLED. The main reason behind the color shift difference is the intrinsic narrow spectra of QLED. This has been double confirmed by the LCD with QD backlight, which also has smaller color shift than LCD with white LED backlight [13]. As for the green and blue colors, we expect that green and blue QLEDs will also have negligible color shift because of their intrinsic narrow spectra. Thus, QLED displays have great potential to overcome the color shift problem.

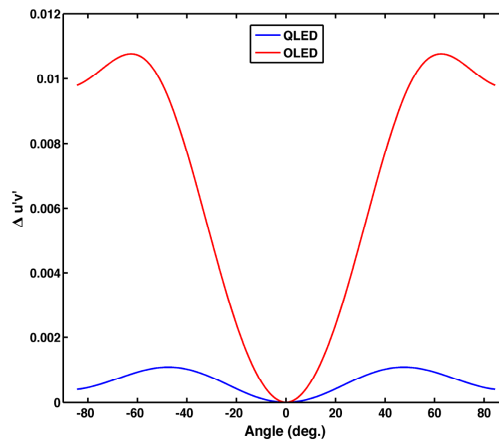


Fig. 13. Calculated color shift of the proposed red QLED and the red OLED.

We also compare the angular emission pattern of our proposed QLED with OLED. Results are shown in Fig. 14. From Fig. 14, the angular emission pattern of our QLED is a little bit closer to the Lambertian light source.

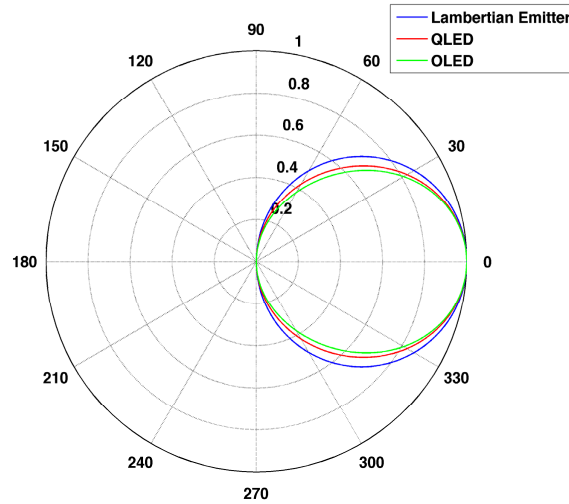


Fig. 14. Simulated angular radiation pattern of the OLED and the QLED structures.

6. Conclusion

We have analyzed the factors affecting the outcoupling of a QLED structure and discussed methods for improving its outcoupling efficiency. By using a high refractive index substrate and optimizing the outcoupling structures, it is possible to enhance the outcoupling efficiency to ~80%. Meanwhile, we have also analyzed the light emitting spectra, color shift, and angular radiation pattern of the QLED structures. Because of its intrinsic narrow emission spectra, QLED structure shows a much weaker color shift as compared to the contemporary OLED structure.

Acknowledgments

The authors are indebted to Prof. Jin Jang from Kyung Hee University for helpful information and thoughtful discussion, Dr. Bert Scholz from Universität Augsburg for helping us with the dipole model, and Dr. Qi Hong and Prof. Yajie Dong of University of Central Florida for the insightful discussion.